

Review

Photocatalytic Water Oxidation on ZnO: A Review

Sharifah Bee Abdul Hamid *, Swe Jyan Teh and Chin Wei Lai

Nanotechnology and Catalysis Research Centre, Institute of Graduate Studies, University of Malaya, 50603 Kuala Lumpur, Malaysia; tehswejyan@gmail.com (S.J.T.); cwlai@um.edu.my (C.W.L.)

* Correspondence: sharifahbee@um.edu.my; Tel.: +60-3-7967-6959

Academic Editor: Yurii V. Geletii

Received: 16 December 2016; Accepted: 2 March 2017; Published: 21 March 2017

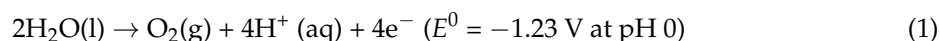
Abstract: The investigation of the water oxidation mechanism on photocatalytic semiconductor surfaces has gained much attention for its potential to unlock the technological limitations of producing H₂ from carbon-free sources, i.e., H₂O. This review seeks to highlight the available scientific and fundamental understanding towards the water oxidation mechanism on ZnO surfaces, as well as present a summary on the modification strategies carried out to increase the photocatalytic response of ZnO.

Keywords: photocatalytic water oxidation; oxygen evolution reaction; photoelectrochemical water-splitting; zinc oxide

1. Introduction

The oxidation of water on the surface of semiconductor photocatalyst materials has attracted much attention for its potential contribution towards the development of efficient artificial photosynthesis and photoelectrochemical (PEC) water-splitting devices. The water oxidation reaction, also known as the oxygen evolution reaction (OER), is the complementary reaction to the hydrogen evolution reaction (HER) in the electrolysis of H₂O. H₂O electrolysis has been considered an attractive source of renewable H₂ [1–4]. PEC water-splitting and artificial photosynthesis devices utilize photocatalytically-active semiconductor materials to absorb solar energy necessary to break the chemical bonds of H₂O. In 1972, the first account on the H₂O photolysis was reported by Fujishima and Honda using n-type titanium dioxide (TiO₂) electrode connected to a platinum black electrode through an external circuit [5]. The innovation by Fujishima and Honda Laboratories produced the first viable PEC water-splitting cell with an approximate quantum efficiency of 0.1%. To date, solar-to-H₂ (STH) efficiencies of 12.7% have been achieved using a p-GaInP₂/GaAs electrode as photoanode [6], and the record has only recently been surpassed at 14% using a Z-scheme tandem cell comprised of Rh-functionalized AlInPO_x photocathode and RuO₂ as photoanode [7].

The decomposition of pure water into H₂ and O₂ itself is not a thermodynamically-favorable process ($\Delta E^0 = -1.23$ V) and requires an external potential bias to drive the uphill reaction. The OER in an electrolytic cell is a four-electron transfer process (Equation (1)) and has been considered the bottleneck in the decomposition of water to gaseous O₂ and H₂ [1]:



Commercial electrolyzers rely on external power sources to supply the required overpotential for water-splitting. The energy consumption of industrial-scale electrolyzers is high due to the energy barriers imposed by cathodic and anodic overpotentials, as well as IR drop between electrodes [8]. Coupling renewable energy sources with electrolyzers has been proposed to be a sustainable approach to utilize excess renewable energy produced at low-demand times of the day. Alternatively, in PEC

water-splitting and artificial photosynthesis devices, the photovoltaic and electrolytic functions are integrated into a single device. Compared to a photovoltaic-electrolyzer unit, PEC water-splitting and artificial photosynthesis devices offer the advantage of minimizing energy loss incurred by transfer of energy between components (i.e., electric supply and electrolyzer). The formation of charged species (electron-hole pairs) via direct conversion of solar energy at the semiconductor-electrolyte interface promotes the water oxidation reaction through the interaction between the electron-deficient hole sites with OH^- ions [9]. The application of photocatalytic semiconductor materials such as ZnO to promote water oxidation reactions have been viewed as a strategy to harvest solar energy directly to operate the PEC water-splitting device.

In the search for suitable transition metal oxide photocatalysts to promote the water oxidation reaction, ZnO has emerged as a leading candidate due to its low toxicity, abundance and straightforward synthesis processes. Nevertheless, the effective implementation of ZnO as water oxidation photocatalyst still requires improved design and synthesis strategies to overcome the limitations of ZnO. Therefore, the active investigation of the mechanism of water oxidation on ZnO surfaces (and metal oxide surfaces in general) is motivated by the opportunity to design and synthesize photocatalyst materials that can operate at acceptable catalytic activities compared to noble metal electrodes (Ru, Ir and Pt), but at the fraction of the cost.

This review seeks to provide the reader with a current understanding of the photocatalytic water oxidation reaction on ZnO surfaces, leading to the identification of critical features and structure of photocatalysts for effective and improved catalyst design. An overview of the photocatalytic water oxidation process specific to ZnO is presented, followed by a summary of current modification approaches to enhance the light-harvesting, charge transport and electrocatalytic properties of ZnO. The review concludes with suggestions for research opportunities in the design and development of OER catalysts.

2. The Mechanism of Photocatalytic Water Oxidation on ZnO

2.1. Photoexcitation and Charge Separation

The photocatalytic reaction taking place at the surface of ZnO, and semiconductor photoanodes in general, involves the absorption of incident photons, the photoexcitation of electron-hole pairs and long-distance transport of charges. Under illumination, ZnO absorbs photons with energies equal to or greater than its band gap of 3.37 eV [10]. For every electron that is photoexcited to the conduction band (CB), an empty state is created in the overlapping oxygen 2p orbitals which make up the valence band (VB). This means that the concentration of free electrons and holes in an illuminated semiconductor are larger than that at dark conditions, with the new steady state described by quasi-Fermi levels.

Subsequently, the photoexcited electrons migrate away from the site of excitation towards the cathode/photocathode in a process called charge separation. The charge separation process is enabled by the formation of depletion layer at the semiconductor-electrolyte interface, which has been well-described in a seminal review on solar water splitting cells [11]. Briefly, when a semiconductor is immersed into an aqueous electrolyte, a potential difference is set up and transfer of charges occur between the electrode and electrolyte until the Fermi levels reach equilibrium [12]. For ZnO, which is an n-type semiconductor, the Fermi level is typically higher than the redox potential of the electrolyte, and hence electrons will be transferred from the electrode into the solution. Therefore, there is a positive charge associated with the space charge region, and this is reflected in an upward bending of the band edges [13]. Thus, when an electron is promoted by photoexcitation, the depletion layer supports the unidirectional flow of photoexcited electrons towards the cathode/photocathode. The positively-charged holes that remain on the surface of the semiconductor act as active sites for subsequent water oxidation steps.

The electron mobility properties of a metal oxide supports effective charge separation following the photoexcitation step. In semiconductors, higher donor concentrations are desirable to allow for long-distance transport of electrons away from the site of photoexcitation and across the bulk material.

The high electron mobility of ZnO may be attributed to its filled d^{10} electron configuration [14,15], leading to a high donor concentration, up to $4 \times 10^{16} \text{ cm}^{-3}$ [16].

Despite possessing higher electron mobility, several studies have shown that ZnO demonstrated a lower photo-conversion efficiency compared to TiO_2 [17,18]. This observation has been attributed to the higher rate of recombination in ZnO compared to TiO_2 [17]. Two different radiative recombination processes were found to be involved in the excitonic emission of ZnO—free exciton recombination (slow) and near surface exciton recombination (fast) [19]. The presence of impurity atoms other than oxygen defects may also change the charge transport properties of ZnO.

The light absorption, photoluminescence properties and charge carrier properties of ZnO were found to be influenced by structural defects in the crystal lattice. In one study, oxygen vacancies and interstitial oxygen defects influenced the photocatalytic activity of ZnO by splitting the IR absorption band and visible photoluminescence emission peak, reporting enhanced charge separation efficiency with increasing oxygen defects [20]. The increase in charge separation efficiency may be attributed to the role of oxygen vacancies as electron acceptors, and interstitial oxygen as a shallow trap for photogenerated holes [21], preventing the recombination of the photogenerated electron–hole species. $\text{Zn}(\text{OH})_2$ species act as deep trapping sites of photoexcited charges, resulting in poor photocatalytic activity [22]. The reader is also referred to a comprehensive review on the influence of doping and native defects on the electrical conductivity and optical properties of ZnO [10].

2.2. Water Oxidation Reactions

The water oxidation process begins with the binding of an OH^- ion to the active catalyst site. There are differing opinions with regards to the actual site of adsorption. The conventional view is that charged OH^- species bind to the metal center. A recent study on iridium-based $\text{La}_2\text{LiIrO}_6$ perovskites as OER catalyst demonstrated that the Ir–O bond was not responsible for bond-breaking activity; rather, the oxygen radicals on the surface of the catalyst acted as electrophilic active sites [23]. These surface oxygen radicals were proposed to participate in the OER mechanism through nucleophilic attack from the water oxygen lone pairs, followed by the removal of H^+ via proton-coupled electron transfer reactions.

H_2O was also found to interact with ZnO through dissociative adsorption [24]. There are two types of sites available for H_2O physisorption on the surface of ZnO, i.e., heterogeneous and homotactic character [25]. The physisorption sites on ZnO possess energies less than 21 kJ/mol H_2O , and chemisorption sites with energies of 84–96 kJ/mol, whereas the enthalpy of H_2O chemisorption on ZnO is -150 ± 10 kJ/mol [26]. The hydroxylated metal oxide surface increases the likelihood to catalyze the dissociation of H_2O , but also affects the material's proton transfer reactivity [27].

Subsequently, a series of proton-coupled electron transfers transform the adsorbed OH^- species to O_2 . In the conventional view on the water oxidation process (Table 1), The M–OH complex (M referring to a metal active site) may decompose to form adsorbed atomic O (Bockris oxide path). Alternatively, the M–OH complex may undergo nucleophilic attack by a hydroxyl, OH^- ion, leading to the formation of either adsorbed species on the active site: (1) atomic O (Krasil'shchikov, Bockris electrochemical oxide path and Kobussen mechanisms); or (2) H_2O_2 (Damjanovic and Hoare mechanisms). H_2O_2 adsorbed on active sites are proposed to decompose to superoxide anions (M-O_2^-). The Kobussen mechanism features both the formation of atomic O and H_2O_2 as a result of the M–O species being subjected to multiple nucleophilic attack reactions.

For semiconductor electrodes, the mobility of adsorbed species is restricted and the formation of M-O_2^- species is favored in order to circumvent the need for atomic rearrangement leading to O–O bond formation. A recent discovery has been made on the mechanism of OER at hematite surfaces: the Fe^{3+} –OH complex undergoes dehydrogenation to form a $\text{Fe}^{4+}=\text{O}$ species before interacting with H_2O to form the Fe^{3+} –O–O–H species [28]. This finding suggests that the formation of Zn–O–O–H species on ZnO may include a dehydrogenation reaction as well. For a summary on the techniques for measuring catalytic activity and kinetics of the OER process, the reader is referred to a review by Fabbri et al. [29].

O₂ may be produced either via: (1) the formation of O-O bond between two M-O species (Damjanovic, Krasil'shchikov, Bockris oxide and Bockris electrochemical oxide mechanisms); or (2) the dissociation of O₂ from the M-O₂⁻ complex (Hoare and Kobussen mechanisms). The former termination mechanism is favored at the surface of metal electrodes as the M-O species is mobile and free to rearrange itself at the surface. As the M-O species on semiconductor surfaces are not mobile, the termination mechanism on semiconductor surfaces follows the latter mechanism.

Table 1. Proposed mechanisms of the oxygen evolution reaction.

Mechanism	Initiation	Intermediate Reactions	Termination
Damjanovic [30]	$M + OH^- \rightarrow MOH + e^-$	$MOH + OH^- \rightarrow MO-H-OH^-$ $MO-H-OH^- \rightarrow MO-H-OH + e^-$ $MO-H-OH \rightarrow MO + H_2O$ $MO + OH^- \rightarrow MHO_2 + e^-$	$MHO_2 + OH^- \rightarrow M + O_2 + H_2O + e^-$ Or: $2MO \rightarrow O_2 + 2M$
Krasil'shchikov [31]	$M + OH^- \rightarrow MOH + e^-$	$MOH + OH^- \rightarrow MO^- + H_2O$ $MO^- \rightarrow MO + e^-$	$2MO \rightarrow O_2 + 2M$
Hoare [32]	$M + OH^- \rightarrow MOH + e^-$	$MOH + OH^- \rightarrow MH_2O_2^-$ $2MH_2O_2^- \rightarrow M + MO_2^- + 2H_2O$	$MO_2^- \rightarrow M + O_2 + 2e^-$
Bockris oxide path [33]	$M + OH^- \rightarrow MOH + e^-$	$2MOH \rightarrow MO + M + H_2O$	$2MO \rightarrow 2M + O_2$
Bockris electrochemical oxide path [33]	$M + OH^- \rightarrow MOH + e^-$	$MOH + OH^- \rightarrow MO + H_2O + e^-$	$2MO \rightarrow 2M + O_2$
Kobussen [34]	$M + OH^- \rightarrow MOH + e^-$	$MOH + OH^- \rightarrow MO + H_2O + e^-$ $MO + OH^- \rightarrow MO_2H^-$ $MO_2H^- + OH^- \rightarrow MO_2^- + H_2O + e^-$	$MO_2^- \rightarrow M + O_2 + e^-$

Based on the available understanding of the OER mechanism, the following steps in the OER process have been identified as the rate-determining step, and catalysis of either step is expected to significantly enhance the rate of OER:

- Ionization of water to OH⁻
- Conversion of OH⁻ to O-O-H species on catalytically-active surface sites
- Desorption of O₂ from catalyst surface

The semiconductor photocatalyst should favor the formation of the M-O-O⁻ /M-O-O-H complex rather than the M-O species for two reasons: (1) the formation of O₂ from the combination of M-O is restricted by the mobility of M-O on the surface of the non-pure metal catalysts; and (2) to suppress the back reaction of H₂ and O₂ recombination.

3. Modifications of ZnO for Enhanced Photocatalytic Water Oxidation Activity

Two main research approaches have emerged in the development of photocatalytic materials with improved photon-to-current conversion efficiency (PCE). The first approach is to tune the electronic structure of ZnO in order to extend its ability to harvest photons in the visible region of the light spectrum (band gap engineering). The light-harvesting ability can be enhanced by controlling the morphology of the ZnO crystal (quantum confinement effect), modifying the carrier concentration within the ZnO crystal lattice (doping), or by functionalizing the surface of ZnO with photosensitizer molecules. The second approach is to promote effective photogenerated charge separation by controlling the defects in the crystal lattice or incorporating electron transfer agents [35]. Alternatively, hybridizing ZnO with metallic or semiconductor co-catalysts has proven successful in accelerating water oxidation reactions. A summary of the various strategies used to enhance the PCE of ZnO is presented in Table 2.

The selection and optimization of ZnO synthesis methods take into consideration the ability to control the size, morphology, and defects within the crystal lattice. Many synthesis methods have been proposed for the synthesis of ZnO nanostructures, with a goal to increase the control of crystal growth at mild operating conditions (e.g., ambient pressure and temperature). Techniques which are able to control the growth of ZnO at the atomic-level include metal-organic chemical vapor deposition

(MO-CVD) [36–38], atomic layer deposition [39,40], laser ablation [41,42] and molecular beam epitaxy [43,44]. Template based synthesis allows for the formation of well-defined structures [45,46]. The wet chemical methods include hydrothermal synthesis [14,47], sol-gel spin-coating [48–51], electrochemical deposition [52–55] and anodization [56].

A variety of ZnO morphologies (nanowires, nanorods, core/shell, nanoflowers) have been encountered in literature. The role of particle morphology on the water oxidation activity and photoabsorption characteristics of ZnO may be attributed to the type and amount of exposed crystal facets, i.e., a greater proportion of exposed polar surfaces were found to enhance the photocatalytic activity of the ZnO [57,58]. It was reported that OH^- ions adsorb preferentially onto the positively-charged [0001]-Zn surface, increasing the rate of interaction between OH^- and holes for accelerated water oxidation reactions [59]. As such, it was postulated that preferential crystal growth leading to a high degree of exposure of the [0001] facets would enhance its catalytic activity. It was found that ZnO nanostructures with a higher exposure of [0001] facet exhibited stronger absorption in 400–450 nm range [60]. In addition, branched structures greatly enhances their surface area, leading to improved light harvesting [61]. ZnO nanostructures with higher aspect ratio show significantly higher photocatalytic performances [62], which indicates that nanoparticles with high aspect ratio, i.e., nanowires, nanotubes and nanorods most likely facilitate charge transport along metal oxide materials with nanometer resolution across micrometer-scale distances [63]. The electron transport through the nanostructure is a crucial aspect to achieve a good photon-to-electron quantum efficiency [64]. Thus, vertically-aligned nanowire or nanorod arrays remain the preferred structural configuration for efficient electron transport in PEC water-splitting.

The carrier concentration of ZnO, and thus photocatalytic activity, may be controlled by manipulating the amount of oxygen defects as well as impurity atoms in the structure. The formation of oxygen vacancies in ZnO were reported to occur as follows [65]: the oxygen atoms escape from the lattice sites due to the low oxygen partial pressure and the high annealing temperature. Subsequently, the escaped oxygen is reduced by H_2 and released in the form of H_2O . The amount of oxygen vacancies was also influenced by the structure of the ZnO crystal, e.g., a greater amount of oxygen vacancies were observed at the surfaces of rod-structured ZnO [66]. Accordingly, the concentration and type of oxygen defects vary according to the synthesis technique and reaction parameters, e.g., choice of solvent [67], synthesis temperature [66], and pressure.

An increase in photocatalytic activity of ZnO with increasing oxygen defects has often been attributed to the role of the oxygen defect to increase charge separation, although the type of oxygen defect has not always been defined specifically. A previous study reporting the synthesis of graphene-hybridized ZnO triangles attributed its increased output photocurrent density of $1.26 \text{ mA}\cdot\text{cm}^{-2}$ (compared to $0.321 \text{ mA}\cdot\text{cm}^{-2}$) to an increase of oxygen defects in the ZnO triangle nanostructure [68]. Other studies have indicated that the presence of oxygen vacancies narrows the band gap of ZnO [69,70], leading to reduced overpotential for photoexcitation of electrons. Thus, the light absorption properties of ZnO is tunable by controlling the intrinsic defect states [71]. The amount of hydroxylated groups terminating at the ZnO surface should be controlled to allow for optimal water dissociation as well as efficient light harvesting.

Other attempts to narrow the band gap of ZnO include doping with metal impurities such as Cu and Mn [72]. The impurities incorporated into the semiconductor can be located at the surface (inhomogeneous doping), or dispersed throughout the electrode material as a solid solution (homogeneous doping). The incorporation of dopant atoms into the semiconductor crystal lattice introduces intermediate energy levels within the intrinsic semiconductor, which lowers the energy requirement for photoexcitation of electrons. Thus, band gap modification can be achieved via creation of oxygen vacancies, non-metal doping, co-doping of non-metals and transition metal doping [73]. Non-metal doping, e.g., nitrogen, carbon or sulfur into ZnO, has been extensively studied with a view to narrowing the bandgap [74]. The narrowing of the band gap using non-metal dopants was previously attributed to the mixing of O 2p states with the dopant's 2p states, thereby forming occupied

states with higher energy in the valence band [75]. The amount of doping and the location of dopants within the crystal structure must be well-controlled in order to achieve high photoelectrochemical performance; overdoping and inappropriate selection of dopants will lead to a reduction in Auger recombination lifetime and the formation of compensating centers, respectively [10].

The addition of photosensitizer nanoparticles to the surface of the semiconductor has been found to effectively improve the photocurrent response of ZnO photoelectrodes. Photosensitizers adsorbed on the photocatalyst utilize visible light to excite electrons, then the excited electrons are injected into the conduction band of the photocatalyst. The photoexcited electrons can then be transferred from the photosensitizer to the active sites on the semiconductor material surface for reaction with redox species to form O₂. Conventional photosensitizers, e.g., dyes, possess poor stability but are valued for their low cost of fabrication. On the other hand, advanced photosensitizers such as CdSe possess broad absorption band and photostability, but with high material and synthesis costs [76].

The second approach to improve the STH efficiency of ZnO photoanodes involves the suppression of electron–hole recombination in ZnO on semiconductor surfaces and improving the capability for instantaneous charge collection, separation, and transportation. Heterostructures formed using metal oxide co-catalysts [77,78] or carbon-based electron transfer agents such as graphene are the most widely investigated materials for improving carrier transport in semiconductors.

The co-catalyst is typically a noble metal or metal oxide or a combination of them, loaded onto the surface of photocatalyst to suppress recombination, enhance charge separation, increase the number of reactive sites and reduce activation energy for gas evolution. In co-catalyst-ZnO hybridized materials, the water oxidation reactions may take place either directly on the surface of ZnO, and/or on the co-catalyst material. The hybridization of two semiconductor materials also leads to the formation of heterojunctions which provide additional advantages in charge transport [79].

The bonding strength between the active site and reactants determines the catalytic activity of a material; interactions that are too strong prevents the desorption of O₂ from the photocatalyst surface and interactions that are too weak prevent the binding of OH[−] to the photocatalyst. For this reason, an optimal binding energy is crucial. The strength of interaction between the active site and the reactant may be tuned by changing the composition of the material, leading to changes in the filling of the bonding and antibonding states, e.g., changing the composition of the material changes the strength of coupling between oxygen 2p states and metal d states [80]. A stronger bond interaction may also be achieved by shifting the energy of antibonding states upwards, relative to the Fermi level.

The application of carbon nanostructures has been a subject of interest, due to the tunable properties, chemical stability (in contrast to metal-based promoters, which suffer from corrosion) and low cost of production. The ability to tune the properties of graphene between a semiconductor and semimetal makes this material such an attractive subject of investigation as a non-metal promoter for electro- and photocatalytic applications [81]. The enhanced photocurrent response in ZnO hybridized with graphene and its derivatives have been variously attributed to its activity as photosensitizer [82] or electron transfer agent [77,83]. Pristine, defect-free graphene is able to behave like a semimetal, making it useful as co-catalyst and electron transfer agent. In this situation, the enhanced performance of ZnO-rGO can be attributed to enhanced charge separation [71]. On the other hand, when graphene is tuned to behave like a semiconductor, it was proposed that it could exhibit photocatalytic or photosensitizer properties [81].

One major challenge in the development of ZnO-based photoanodes for water oxidation is related to its chemical stability. Electrolyte solutions containing alkaline electrolytes, e.g., KOH and NaOH promote the rate of water oxidation reaction by providing an excess of OH[−] ions, thereby reducing the IR drop caused by ion transport. When immersed in alkaline solutions, the ZnO surface is transformed to Zn(OH)₂ and the rate of transformation increases with increasing pH. Zn(OH)₂ will further dissolve into Zn²⁺ ions due to the presence of OH[−] ions to reduce Zn(OH)₂. Additionally, ZnO experiences a decrease in the photostability of ZnO under prolonged light irradiation, due to photocorrosion mechanisms [84,85]. Therefore, to enhance its photocatalytic efficiency, it is of crucial importance to design strategies which can suppress the recombination of electron–hole pairs and photocorrosion of ZnO.

Table 2. Summary of modification strategies to enhance ZnO photocurrent density. SCE, Saturated Calomel Electrode; RHE, Reversible Hydrogen Electrode; MWCNT, Multi-Walled Carbon Nanotubes.

Structure	Preparation Method	Enhancement Strategy	Electrolyte	Reference Electrode	Photocurrent Density ($\text{mA}\cdot\text{cm}^{-2}$)			Reference
					Applied Potential (V)	Control Electrode	Modified Electrode	
ZnO nanorods	Electrochemical deposition + photochemical deposition	Cobalt phosphate co-catalyst	0.1 M K_3PO_4	Ag/AgCl	0	0.009	0.023	[86]
ZnO nanorod @nanoplatelet core-shell array	Hydrothermal + photoreduction	Au co-catalyst	0.5 M Na_2SO_4	SCE	0.6	0.01	0.06	[87]
ZnO film	Electron-beam glancing angle deposition	Crystal growth method	0.5 M NaClO_4	Ag/AgCl	1	0.045	0.142	[88]
ZnO nanowires	Hydrothermal + sol-gel	TiO_2 heterojunction	0.1 M NaOH	RHE	0.85	0.08	0.19	[89]
ZnO nanorods	Hydrothermal	MWCNT hybridization	0.5 M Na_2SO_4	Ag/AgCl	0	0.06	0.25	[83]
ZnO nanorods	Hydrothermal + electron beam evaporation	Ag co-catalyst	0.5 M Na_2SO_4	Ag/AgCl	0	0.089	0.325	[90]
ZnO nanowires	Hydrothermal	Graphene quantum dot photosensitizer	0.5 M Na_2SO_4	-	0.6	0.11	0.34	[82]
ZnO film	Spray pyrolysis	Cu-doping	0.5 M NaOH	SCE	0.6	0.05	0.35	[91]
ZnO nanowires	Hydrothermal	N-Doping	0.5 M NaClO_4	Ag/AgCl	1	0.017	0.4	[92]
ZnO nanowires	Hydrothermal	MWCNT hybridization	0.1 M Na_2SO_4	Ag/AgCl	0	0.05	0.4	[93]
ZnO nanorods	Ammonia-assisted hydrolysis	Surfactant mediated crystal growth	0.1 M LiI 0.05 M I_2 0.5 M TBP	-	0	0.37	0.47	[94]
ZnO nanowires	Hydrothermal + atomic layer deposition	TiO_2 heterojunction	0.1 M KOH	Ag/AgCl	0.25	0.4	0.5	[95]
ZnO nanosheets	Electrodeposition	Exposed polar facet	0.5 M Na_2SO_4	Ag/AgCl	1	0.2	0.51	[96]
ZnO nanotubes	Anodization	Control of morphology	0.5 M Na_2SO_4	SCE	0.25	0.25	0.52	[97]
ZnO nanorods	Chemical bath deposition + photodeposition	Cobalt phosphate co-catalyst	0.1 M KH_2PO_4	SCE	0.5	0.36	0.54	[98]
ZnO nanorods	Spin-coating	Cu-doping	0.1 M NaOH	SCE	0	0.312	0.752	[99]
Fe_3O_4 -ZnO core-shell	Hydrothermal	Fe_3O_4 heterojunction + rGO hybridization	0.1 M KOH	RHE	1.23	0.52	0.85	[78]

Table 2. Cont.

Structure	Preparation Method	Enhancement Strategy	Electrolyte	Reference Electrode	Photocurrent Density ($\text{mA}\cdot\text{cm}^{-2}$)			Reference
					Applied Potential (V)	Control Electrode	Modified Electrode	
ZnO nanotetrapods	Thermal evaporation + chemical bath deposition	Morphology + N-doping	0.5 M Na_2SO_4	RHE	0.92	0.046	0.99	[100]
ZnO triangles	Hydrothermal	Control of morphology + graphene oxide hybridization	1.0 M NaOH	RHE	1.23	0.321	1.29	[68]
ZnO nanoparticles	Spin coating	Effect of annealing temperature	0.1 M NaOH	SCE	0	0.105	1.321	[101]
ZnO nanowires/ RGO/ ZnIn_2S_4	Hydrothermal	Heterojunction + ZnIn_2S_4 photosensitizer	1.0 M Na_2SO_4	Ag/AgCl	0.5	0.6	1.41	[102]
ZnO nanopencil arrays	Hydrothermal + photoreduction	Au photosensitiser	0.5 M Na_2SO_4	Ag/AgCl	1	0.7	1.5	[103]
ZnO nanorod	Electrodeposition	rGO hybridization	0.1 M KOH	Ag/AgCl	1	1	1.8	[104]
ZnO nanowires	Hydrothermal + wet chemical impregnation	CdTe quantum dot photosensitiser	0.5 M Na_2SO_4	Ag/AgCl	1	0.7	2	[105]
ZnO nanowires	Sol-gel spin coating + electrochemical deposition	Au co-catalyst	0.1 M NaOH	SCE	0.5	1.5	2.6	[106]
ZnO nanorods	Hydrothermal + ion exchange	AgSbS_2 co-catalyst	1.0 M Na_2S	Ag/AgCl	+0.212 (Control)+0.096 (Modified)	0.41	5.08	[77]
ZnO nanorod	Electrodeposition	Effect of applied potential	1.0 M NaOH 1 wt % ethylene glycol	SCE	1	5.74	12.94	[107]

4. Conclusions

Various modification strategies have been proposed to enhance the activity of ZnO (and semiconductor metal oxides in general) towards photocatalytic water oxidation. Nevertheless, the challenge remains to identify affordable synthesis techniques that can provide fine control over the morphology, carrier concentration and bonding between ZnO and extrinsic modifiers (photosensitizers and co-catalysts). The modifications made to ZnO need to be optimized such that the catalyst achieves the following goals:

1. Increased solar harvesting and photon-to-current conversion efficiency
2. The position of the valence band is more negative compared to the OH^-/O_2 redox couple potential (so that an external potential bias would not be necessary)
3. The OER proceeds at minimum overvoltage
4. Corrosion is suppressed

Research that can further elucidate the OER mechanism and conclusively identify the nature of the catalytically active site on ZnO remains in great demand. Thus, it becomes necessary to develop innovative analytical in-situ techniques that can detect transient intermediate species. The insights gained from the study of photocatalytic water oxidation on the surface of ZnO will undoubtedly contribute towards the overall growth of sustainable technologies to obtain H_2 from carbon-free sources.

Acknowledgments: The authors wish to thank the University of Malaya for their generous support through the Grand Challenge initiative (grant No. GC001A-14AET), Fundamental Research Grant Scheme (FP008-2015A) and Postgraduate Research Grant (PG221-2016A).

Author Contributions: Sharifah Bee Abdul Hamid conceived the scope and aim of the paper and contributed towards data analysis and discussion; Swe Jyan Teh collected the data and wrote the paper; Chin Wei Lai contributed towards critical revision of the paper.

Conflicts of Interest: The authors declare no conflict of interest.

References

1. Kreuter, W.; Hofmann, H. Electrolysis: The important energy transformer in a world of sustainable energy. *Int. J. Hydrogen Energy* **1998**, *23*, 661–666. [[CrossRef](#)]
2. Ursua, A.; Gandia, L.M.; Sanchis, P. Hydrogen production from water electrolysis: Current status and future trends. *Proc. IEEE* **2012**, *100*, 410–426. [[CrossRef](#)]
3. Xiang, C.; Papadantonakis, K.M.; Lewis, N.S. Principles and implementations of electrolysis systems for water splitting. *Mater. Horiz.* **2016**, *3*, 169–173. [[CrossRef](#)]
4. Zeng, K.; Zhang, D. Recent progress in alkaline water electrolysis for hydrogen production and applications. *Prog. Energy Combust. Sci.* **2010**, *36*, 307–326. [[CrossRef](#)]
5. Fujishima, A.; Honda, K. Electrochemical photolysis of water at a semiconductor electrode. *Nature* **1972**, *238*, 37–38. [[CrossRef](#)] [[PubMed](#)]
6. Khaselev, O.; Turner, J.A. A monolithic photovoltaic-photoelectrochemical device for hydrogen production via water splitting. *Science* **1998**, *280*, 425–427. [[CrossRef](#)] [[PubMed](#)]
7. May, M.M.; Lewerenz, H.-J.; Lackner, D.; Dimroth, F.; Hannappel, T. Efficient direct solar-to-hydrogen conversion by in situ interface transformation of a tandem structure. *Nat. Comm.* **2015**, *6*, 8286. [[CrossRef](#)] [[PubMed](#)]
8. Mori, M.; Mržljak, T.; Drobnič, B.; Sekavčnik, M. Integral characteristics of hydrogen production in alkaline electrolyzers. *Stroj. Vestn. J. Mech. Eng.* **2013**, *59*, 585–594. [[CrossRef](#)]
9. Van de Krol, R. Principles of photoelectrochemical cells. In *Photoelectrochemical Hydrogen Production*; van de Krol, R., Grätzel, M., Eds.; Springer: Boston, MA, USA, 2012; pp. 13–67.
10. Janotti, A.; Van de Walle, C.G. Fundamentals of zinc oxide as a semiconductor. *Rep. Prog. Phys.* **2009**, *72*, 126501. [[CrossRef](#)]
11. Walter, M.G.; Warren, E.L.; McKone, J.R.; Boettcher, S.W.; Mi, Q.; Santori, E.A.; Lewis, N.S. Solar water splitting cells. *Chem. Rev.* **2010**, *110*, 6446–6473. [[CrossRef](#)] [[PubMed](#)]

12. Gratzel, M. Photoelectrochemical cells. *Nature* **2001**, *414*, 338–344. [[CrossRef](#)] [[PubMed](#)]
13. Zhang, Z.; Yates, J.T. Band bending in semiconductors: Chemical and physical consequences at surfaces and interfaces. *Chem. Rev.* **2012**, *112*, 5520–5551. [[CrossRef](#)]
14. Jayah, N.A.; Yahaya, H.; Mahmood, M.R.; Terasako, T.; Yasui, K.; Hashim, A.M. High electron mobility and low carrier concentration of hydrothermally grown ZnO thin films on seeded a-plane sapphire at low temperature. *Nanoscale Res. Lett.* **2015**, *10*, 1–10. [[CrossRef](#)] [[PubMed](#)]
15. Inoue, Y. Photocatalytic water splitting by RuO₂-loaded metal oxides and nitrides with d⁰- and d¹⁰-related electronic configurations. *Energy Environ. Sci.* **2009**, *2*, 364–386. [[CrossRef](#)]
16. Look, D.C. Recent advances in ZnO materials and devices. *Mater. Sci. Eng. B* **2001**, *80*, 383–387. [[CrossRef](#)]
17. Chandiran, A.K.; Abdi-Jalebi, M.; Nazeeruddin, M.K.; Grätzel, M. Analysis of electron transfer properties of ZnO and TiO₂ photoanodes for dye-sensitized solar cells. *ACS Nano* **2014**, *8*, 2261–2268. [[CrossRef](#)] [[PubMed](#)]
18. Hernandez, S.; Hidalgo, D.; Sacco, A.; Chiodoni, A.; Lamberti, A.; Cauda, V.; Tresso, E.; Saracco, G. Comparison of photocatalytic and transport properties of TiO₂ and ZnO nanostructures for solar-driven water splitting. *Phys. Chem. Chem. Phys.* **2015**, *17*, 7775–7786. [[CrossRef](#)] [[PubMed](#)]
19. Xiong, G.; Pal, U.; Serrano, J.G. Correlations among size, defects, and photoluminescence in ZnO nanoparticles. *J. Appl. Phys.* **2007**, *101*, 024317. [[CrossRef](#)]
20. Zheng, Y.; Chen, C.; Zhan, Y.; Lin, X.; Zheng, Q.; Wei, K.; Zhu, J.; Zhu, Y. Luminescence and photocatalytic activity of ZnO nanocrystals: Correlation between structure and property. *Inorg. Chem.* **2007**, *46*, 6675–6682. [[CrossRef](#)] [[PubMed](#)]
21. Djurišić, A.B.; Leung, Y.H. Optical properties of ZnO nanostructures. *Small* **2006**, *2*, 944–961. [[CrossRef](#)] [[PubMed](#)]
22. Baek, M.; Kim, D.; Yong, K. Simple but effective way to enhance photoelectrochemical solar-water-splitting performance of ZnO nanorod arrays: Charge-trapping Zn(OH)₂ annihilation and oxygen vacancy generation by vacuum annealing. *ACS Appl. Mater. Interfaces* **2017**, *9*, 2317–2325. [[CrossRef](#)] [[PubMed](#)]
23. Grimaud, A.; Demortiere, A.; Saubanere, M.; Dachraoui, W.; Duchamp, M.; Doublet, M.-L.; Tarascon, J.-M. Activation of surface oxygen sites on an iridium-based model catalyst for the oxygen evolution reaction. *Nat. Energy* **2016**, *2*, 16189. [[CrossRef](#)]
24. Gouvêa, D.; Ushakov, S.V.; Navrotsky, A. Energetics of CO₂ and H₂O adsorption on zinc oxide. *Langmuir* **2014**, *30*, 9091–9097. [[CrossRef](#)] [[PubMed](#)]
25. Nagao, M. Physisorption of water on zinc oxide surface. *J. Phys. Chem.* **1971**, *75*, 3822–3828. [[CrossRef](#)]
26. Low, M.J.D.; Taylor, H.A. The adsorption of water and carbon monoxide by zinc oxide. *J. Phys. Chem.* **1959**, *63*, 1317–1318. [[CrossRef](#)]
27. Raymand, D.; van Duin, A.C.T.; Goddard, W.A.; Hermansson, K.; Spångberg, D. Hydroxylation structure and proton transfer reactivity at the zinc oxide–water interface. *J. Phys. Chem. C* **2011**, *115*, 8573–8579. [[CrossRef](#)]
28. Zandi, O.; Hamann, T.W. Determination of photoelectrochemical water oxidation intermediates on haematite electrode surfaces using operando infrared spectroscopy. *Nat. Chem.* **2016**, *8*, 778–783. [[CrossRef](#)] [[PubMed](#)]
29. Fabbri, E.; Habereder, A.; Waltar, K.; Kotz, R.; Schmidt, T.J. Developments and perspectives of oxide-based catalysts for the oxygen evolution reaction. *Catal. Sci. Technol.* **2014**, *4*, 3800–3821. [[CrossRef](#)]
30. Damjanovic, A.; Dey, A.; Bockris, J.O.M. Electrode kinetics of oxygen evolution and dissolution on Rh, Ir, and Pt-Rh alloy electrodes. *J. Electrochem. Soc.* **1966**, *113*, 739–746. [[CrossRef](#)]
31. Krasil'shchikov, A.I. On the intermediate stages of anodic oxygen evolution. *Zh. Fiz. Khim.* **1963**, *37*, 531–537.
32. Hoare, J.P. Oxygen electrode on noble metals. In *Advances in Electrochemical Sciences and Engineering*; Delahay, P., Ed.; Wiley-Interscience: New York, NY, USA, 1967; pp. 201–288.
33. Bockris, J.O.M.; Otagawa, T. The electrocatalysis of oxygen evolution on perovskites. *J. Electrochem. Soc.* **1984**, *131*, 290–302. [[CrossRef](#)]
34. Kobussen, A.G.C.; Broers, G.H.J. The oxygen evolution on La_{0.5}Ba_{0.5}CoO₃. *J. Electroanal. Chem.* **1981**, *126*, 221–240. [[CrossRef](#)]
35. Chen, H.M.; Chen, C.K.; Liu, R.-S.; Zhang, L.; Zhang, J.; Wilkinson, D.P. Nano-architecture and material designs for water splitting photoelectrodes. *Chem. Soc. Rev.* **2012**, *41*, 5654–5671. [[CrossRef](#)] [[PubMed](#)]
36. Galoppini, E.; Rochford, J.; Chen, H.; Saraf, G.; Lu, Y.; Hagfeldt, A.; Boschloo, G. Fast electron transport in metal organic vapor deposition grown dye-sensitized ZnO nanorod solar cells. *J. Phys. Chem. B* **2006**, *110*, 16159–16161. [[CrossRef](#)] [[PubMed](#)]

37. Shi, Z.; Wu, B.; Cai, X.; Xia, X.; Zhang, S.; Yin, W.; Wang, H.; Wang, J.; Dong, X.; Zhang, Y.; et al. Photofacilitated controllable growth of ZnO films using photoassisted metal organic chemical vapor deposition. *Cryst. Growth Des.* **2012**, *12*, 4417–4424. [[CrossRef](#)]
38. Minegishi, K.; Koivai, Y.; Kikuchi, Y.; Yano, K.; Kasuga, M.; Shimizu, A. Growth of p-type zinc oxide films by chemical vapor deposition. *Jpn. J. Appl. Phys.* **1997**, *36*, L1453. [[CrossRef](#)]
39. Bang, S.; Lee, S.; Ko, Y.; Park, J.; Shin, S.; Seo, H.; Jeon, H. Photocurrent detection of chemically tuned hierarchical ZnO nanostructures grown on seed layers formed by atomic layer deposition. *Nanoscale Res. Lett.* **2012**, *7*, 290. [[CrossRef](#)] [[PubMed](#)]
40. Ai, Z.W.; Wu, Y.; Wu, H.; Wang, T.; Chen, C.; Xu, Y.; Liu, C. Enhanced band-edge photoluminescence from ZnO-passivated ZnO nanoflowers by atomic layer deposition. *Nanoscale Res. Lett.* **2013**, *8*, 105. [[CrossRef](#)] [[PubMed](#)]
41. Desarkar, H.S.; Kumbhakar, P.; Mitra, A.K. One-step synthesis of Zn/ZnO hollow nanoparticles by the laser ablation in liquid technique. *Laser Phys Lett.* **2013**, *10*, 055903. [[CrossRef](#)]
42. Usui, H.; Shimizu, Y.; Sasaki, T.; Koshizaki, N. Photoluminescence of ZnO nanoparticles prepared by laser ablation in different surfactant solutions. *J. Phys. Chem. B* **2005**, *109*, 120–124. [[CrossRef](#)] [[PubMed](#)]
43. Matthias, O.; Stephan, G.; Matthias, A.; Thomas, B.; Rudolf, G. Laser molecular beam epitaxy of ZnO thin films and heterostructures. *J. Phys. D* **2014**, *47*, 034002.
44. Adolph, D.; Zamani, R.R.; Dick, K.A.; Ive, T. Hybrid ZnO/GaN distributed Bragg reflectors grown by plasma-assisted molecular beam epitaxy. *APL Mater.* **2016**, *4*, 086106. [[CrossRef](#)]
45. Lai, M.; Riley, D.J. Templated electrosynthesis of zinc oxide nanorods. *Chem. Mater.* **2006**, *18*, 2233–2237. [[CrossRef](#)]
46. Sarkar, K.; Rawolle, M.; Herzig, E.M.; Wang, W.; Buffet, A.; Roth, S.V.; Müller-Buschbaum, P. Custom-made morphologies of ZnO nanostructured films templated by a poly(styrene-block-ethylene oxide) diblock copolymer obtained by a sol–gel technique. *ChemSusChem* **2013**, *6*, 1414–1424. [[CrossRef](#)] [[PubMed](#)]
47. Baruah, S.; Dutta, J. Hydrothermal growth of ZnO nanostructures. *Sci. Tech. Adv. Mater.* **2009**, *10*, 013001–013018. [[CrossRef](#)] [[PubMed](#)]
48. Znaidi, L. Sol–gel-deposited ZnO thin films: A review. *Mater. Sci. Eng. B* **2010**, *174*, 18–30. [[CrossRef](#)]
49. Guo, D.; Sato, K.; Hibino, S.; Takeuchi, T.; Bessho, H.; Kato, K. Low-temperature preparation of (002)-oriented ZnO thin films by sol–gel method. *Thin Solid Films* **2014**, *550*, 250–258. [[CrossRef](#)]
50. Pathak, T.K.; Kumar, V.; Purohit, L.P. High quality nitrogen-doped zinc oxide thin films grown on ITO by sol–gel method. *Physica E* **2015**, *74*, 551–555. [[CrossRef](#)]
51. Valverde-Aguilar, G.; Manríquez Zepeda, J.L. Photoluminescence and photoconductivity studies on amorphous and crystalline ZnO thin films obtained by sol–gel method. *Appl. Phys. A* **2015**, *118*, 1305–1313. [[CrossRef](#)]
52. Postels, B.; Bakin, A.; Wehmann, H.-H.; Suleiman, M.; Weimann, T.; Hinze, P.; Waag, A. Electrodeposition of ZnO nanorods for device application. *Appl. Phys. A* **2008**, *91*, 595–599. [[CrossRef](#)]
53. Fu, M.; Zhou, J. Mechanism of the electrodeposition of ZnO nanosheets below room temperature. *J. Electrochem. Soc.* **2010**, *157*, D450–D453. [[CrossRef](#)]
54. Cruickshank, A.C.; Tay, S.E.R.; Illy, B.N.; Da Campo, R.; Schumann, S.; Jones, T.S.; Heutz, S.; McLachlan, M.A.; McComb, D.W.; Riley, D.J.; et al. Electrodeposition of ZnO nanostructures on molecular thin films. *Chem. Mater.* **2011**, *23*, 3863–3870. [[CrossRef](#)]
55. Skompska, M.; Zarebska, K. Electrodeposition of ZnO nanorod arrays on transparent conducting substrates—A review. *Electrochim. Acta* **2014**, *127*, 467–488. [[CrossRef](#)]
56. Dong, J.; Liu, Z.; Dong, J.; Ariyanti, D.; Niu, Z.; Huang, S.; Zhang, W.; Gao, W. Self-organized ZnO nanorods prepared by anodization of zinc in NaOH electrolyte. *RSC Adv.* **2016**, *6*, 72968–72974. [[CrossRef](#)]
57. Jang, E.S.; Won, J.H.; Hwang, S.J.; Choy, J.H. Fine tuning of the face orientation of ZnO crystals to optimize their photocatalytic activity. *Adv. Mater.* **2006**, *18*, 3309–3312. [[CrossRef](#)]
58. McLaren, A.; Valdes-Solis, T.; Li, G.; Tsang, S.C. Shape and size effects of ZnO nanocrystals on photocatalytic activity. *J. Am. Chem. Soc.* **2009**, *131*, 12540–12541. [[CrossRef](#)] [[PubMed](#)]
59. Dodd, A.; McKinley, A.; Tsuzuki, T.; Saunders, M. Tailoring the photocatalytic activity of nanoparticulate zinc oxide by transition metal oxide doping. *Mater. Chem. Phys.* **2009**, *114*, 382–386. [[CrossRef](#)]

60. He, S.; Zhang, S.; Lu, J.; Zhao, Y.; Ma, J.; Wei, M.; Evans, D.G.; Duan, X. Enhancement of visible light photocatalysis by grafting ZnO nanoplatelets with exposed (0001) facets onto a hierarchical substrate. *Chem. Commun.* **2011**, *47*, 10797–10799. [[CrossRef](#)] [[PubMed](#)]
61. Baxter, J.B.; Aydil, E.S. Dye-sensitized solar cells based on semiconductor morphologies with ZnO nanowires. *Sol. Energy Mat. Sol. Cells* **2006**, *90*, 607–622. [[CrossRef](#)]
62. Zhang, X.; Qin, J.; Xue, Y.; Yu, P.; Zhang, B.; Wang, L.; Liu, R. Effect of aspect ratio and surface defects on the photocatalytic activity of ZnO nanorods. *Sci. Rep.* **2014**, *4*, 4596. [[CrossRef](#)] [[PubMed](#)]
63. Warren, S.C.; Voitchovsky, K.; Dotan, H.; Leroy, C.M.; Cornuz, M.; Stellacci, F.; Hébert, C.; Rothschild, A.; Grätzel, M. Identifying champion nanostructures for solar water-splitting. *Nat. Mater.* **2013**, *12*, 842–849. [[CrossRef](#)] [[PubMed](#)]
64. Kamat, P.V. Manipulation of charge transfer across semiconductor interface. A criterion that cannot be ignored in photocatalyst design. *J. Phys. Chem. Lett.* **2012**, *3*, 663–672. [[CrossRef](#)] [[PubMed](#)]
65. Kim, Y.; Kang, S. Calculation of formation energy of oxygen vacancy in ZnO based on photoluminescence measurements. *J. Phys. Chem. B* **2010**, *114*, 7874–7878. [[CrossRef](#)] [[PubMed](#)]
66. Ullattil, S.G.; Periyat, P.; Naufal, B.; Lazar, M.A. Self-doped ZnO microrods—High temperature stable oxygen deficient platforms for solar photocatalysis. *Ind. Eng. Chem. Res.* **2016**, *55*, 6413–6421. [[CrossRef](#)]
67. Wang, J.; Liu, P.; Fu, X.; Li, Z.; Han, W.; Wang, X. Relationship between oxygen defects and the photocatalytic property of ZnO nanocrystals in Nafion membranes. *Langmuir* **2009**, *25*, 1218–1223. [[CrossRef](#)] [[PubMed](#)]
68. Chandrasekaran, S.; Chung, J.S.; Kim, E.J.; Hur, S.H. Exploring complex structural evolution of graphene oxide/ZnO triangles and its impact on photoelectrochemical water splitting. *Chem. Eng. J.* **2016**, *290*, 465–476. [[CrossRef](#)]
69. Ansari, S.A.; Khan, M.M.; Kalathil, S.; Nisar, A.; Lee, J.; Cho, M.H. Oxygen vacancy induced band gap narrowing of ZnO nanostructures by an electrochemically active biofilm. *Nanoscale* **2013**, *5*, 9238–9246. [[CrossRef](#)] [[PubMed](#)]
70. Wang, J.; Wang, Z.; Huang, B.; Ma, Y.; Liu, Y.; Qin, X.; Zhang, X.; Dai, Y. Oxygen vacancy induced band-gap narrowing and enhanced visible light photocatalytic activity of ZnO. *ACS Appl. Mater. Interfaces* **2012**, *4*, 4024–4030. [[CrossRef](#)] [[PubMed](#)]
71. Kavitha, M.K.; Gopinath, P.; John, H. Reduced graphene oxide-ZnO self-assembled films: Tailoring the visible light photoconductivity by the intrinsic defect states in ZnO. *Phys. Chem. Chem. Phys.* **2015**, *17*, 14647–14655. [[CrossRef](#)] [[PubMed](#)]
72. Kamarulzaman, N.; Kasim, M.F.; Rusdi, R. Band gap narrowing and widening of ZnO nanostructures and doped materials. *Nanoscale Res. Lett.* **2015**, *10*, 346. [[CrossRef](#)] [[PubMed](#)]
73. Rehman, S.; Ullah, R.; Butt, A.M.; Gohar, N.D. Strategies of making TiO₂ and ZnO visible light active. *J. Hazard. Mater.* **2009**, *170*, 560–569. [[CrossRef](#)] [[PubMed](#)]
74. Yu, W.; Zhang, J.; Peng, T. New insight into the enhanced photocatalytic activity of N-, C- and S-doped ZnO photocatalysts. *Appl. Catal. B* **2016**, *181*, 220–227. [[CrossRef](#)]
75. Liu, G.; Wang, L.; Yang, H.G.; Cheng, H.-M.; Lu, G.Q. Titania-based photocatalysts-crystal growth, doping and heterostructuring. *J. Mater. Chem.* **2010**, *20*, 831–843. [[CrossRef](#)]
76. Swiegers, G.F.; MacFarlane, D.R.; Officer, D.L.; Ballantyne, A.; Boskovic, D.; Chen, J.; Dismukes, G.C.; Gardner, G.P.; Hocking, R.K.; Smith, P.F.; et al. Towards hydrogen energy: Progress on catalysts for water splitting. *Aust. J. Chem.* **2012**, *65*, 577–582. [[CrossRef](#)]
77. Han, J.; Liu, Z.; Guo, K.; Zhang, X.; Hong, T.; Wang, B. AgSbS₂ modified ZnO nanotube arrays for photoelectrochemical water splitting. *Appl. Catal. B* **2015**, *179*, 61–68. [[CrossRef](#)]
78. Yusoff, N.; Kumar, S.V.; Pandikumar, A.; Huang, N.M.; Marlinda, A.R.; An'amt, M.N. Core-shell Fe₃O₄-ZnO nanoparticles decorated on reduced graphene oxide for enhanced photoelectrochemical water splitting. *Ceram. Int.* **2015**, *41*, 5117–5128. [[CrossRef](#)]
79. Moniz, S.J.A.; Shevlin, S.A.; Martin, D.J.; Guo, Z.-X.; Tang, J. Visible-light driven heterojunction photocatalysts for water splitting—A critical review. *Energy Environ. Sci.* **2015**, *8*, 731–759. [[CrossRef](#)]
80. Stamenkovic, V.; Mun, B.S.; Mayrhofer, K.J.J.; Ross, P.N.; Markovic, N.M.; Rossmeisl, J.; Greeley, J.; Nørskov, J.K. Changing the activity of electrocatalysts for oxygen reduction by tuning the surface electronic structure. *Angew. Chem. Int. Ed.* **2006**, *118*, 2963–2967. [[CrossRef](#)]
81. Xie, G.; Zhang, K.; Guo, B.; Liu, Q.; Fang, L.; Gong, J.R. Graphene-based materials for hydrogen generation from light-driven water splitting. *Adv. Mater.* **2013**, *25*, 3820–3839. [[CrossRef](#)] [[PubMed](#)]

82. Guo, C.X.; Dong, Y.; Yang, H.B.; Li, C.M. Graphene quantum dots as a green sensitizer to functionalize ZnO nanowire arrays on F-doped SnO₂ glass for enhanced photoelectrochemical water splitting. *Adv. Energy Mater.* **2013**, *3*, 997–1003. [[CrossRef](#)]
83. Tian, J.; Liu, S.; Li, H.; Wang, L.; Zhang, Y.; Luo, Y.; Asiri, A.M.; Al-Youbi, A.O.; Sun, X. One-step preparation of ZnO nanoparticle-decorated reduced graphene oxide composites and their application to photocurrent generation. *RSC Adv.* **2012**, *2*, 1318–1321. [[CrossRef](#)]
84. Sapkal, R.T.; Shinde, S.S.; Waghmode, T.R.; Govindwar, S.P.; Rajpure, K.Y.; Bhosale, C.H. Photo-corrosion inhibition and photoactivity enhancement with tailored zinc oxide thin films. *J. Photochem. Photobiol. B* **2012**, *110*, 15–21. [[CrossRef](#)] [[PubMed](#)]
85. Rudd, A.L.; Breslin, C.B. Photo-induced dissolution of zinc in alkaline solutions. *Electrochim. Acta* **2000**, *45*, 1571–1579. [[CrossRef](#)]
86. Steinmiller, E.M.P.; Choi, K.-S. Photochemical deposition of cobalt-based oxygen evolving catalyst on a semiconductor photoanode for solar oxygen production. *Proc. Natl. Acad. Sci. USA* **2009**, *106*, 20633–20636. [[CrossRef](#)] [[PubMed](#)]
87. Zhang, C.; Shao, M.; Ning, F.; Xu, S.; Li, Z.; Wei, M.; Evans, D.G.; Duan, X. Au nanoparticles sensitized ZnO nanorod@nanoplatelet core-shell arrays for enhanced photoelectrochemical water splitting. *Nano Energy* **2015**, *12*, 231–239. [[CrossRef](#)]
88. Wolcott, A.; Smith, W.A.; Kuykendall, T.R.; Zhao, Y.; Zhang, J.Z. Photoelectrochemical study of nanostructured ZnO thin films for hydrogen generation from water splitting. *Adv. Funct. Mater.* **2009**, *19*, 1849–1856. [[CrossRef](#)]
89. Hernández, S.; Cauda, V.; Chiodoni, A.; Dallorto, S.; Sacco, A.; Hidalgo, D.; Celasco, E.; Pirri, C.F. Optimization of 1D ZnO@TiO₂ core-shell nanostructures for enhanced photoelectrochemical water splitting under solar light illumination. *ACS Appl. Mater. Interfaces* **2014**, *6*, 12153–12167. [[CrossRef](#)] [[PubMed](#)]
90. Wei, Y.; Ke, L.; Kong, J.; Liu, H.; Jiao, Z.; Lu, X.; Du, H.; Sun, X.W. Enhanced photoelectrochemical water-splitting effect with a bent ZnO nanorod photoanode decorated with Ag nanoparticles. *Nanotechnology* **2012**, *23*, 235401. [[CrossRef](#)] [[PubMed](#)]
91. Dom, R.; Baby, L.R.; Kim, H.G.; Borse, P.H. Enhanced solar photoelectrochemical conversion efficiency of ZnO:Cu electrodes for water-splitting application. *Int. J. Photoenergy* **2013**, *2013*, 928321. [[CrossRef](#)]
92. Yang, X.; Wolcott, A.; Wang, G.; Sobo, A.; Fitzmorris, R.C.; Qian, F.; Zhang, J.Z.; Li, Y. Nitrogen-doped ZnO nanowire arrays for photoelectrochemical water splitting. *Nano Lett.* **2009**, *9*, 2331–2336. [[CrossRef](#)] [[PubMed](#)]
93. Zhang, L.; Cheng, H.; Zong, R.; Zhu, Y. Photocorrosion suppression of ZnO nanoparticles via hybridization with graphite-like carbon and enhanced photocatalytic activity. *J. Phys. Chem. C* **2009**, *113*, 2368–2374. [[CrossRef](#)]
94. Rahman, M.Y.A.; Umar, A.A.; Taslim, R.; Salleh, M.M. Effect of surfactant on the physical properties of ZnO nanorods and the performance of ZnO photoelectrochemical cell. *J. Exp. Nanosci.* **2015**, *10*, 599–609. [[CrossRef](#)]
95. Liu, M.; Nam, C.-Y.; Black, C.T.; Kamcev, J.; Zhang, L. Enhancing water splitting activity and chemical stability of zinc oxide nanowire photoanodes with ultrathin titania shells. *J. Phys. Chem. C* **2013**, *117*, 13396–13402. [[CrossRef](#)]
96. Hsu, Y.-K.; Lin, Y.-G.; Chen, Y.-C. Polarity-dependent photoelectrochemical activity in ZnO nanostructures for solar water splitting. *Electrochem. Commun.* **2011**, *13*, 1383–1386. [[CrossRef](#)]
97. Faid, A.Y.; Allam, N.K. Stable solar-driven water splitting by anodic ZnO nanotubular semiconducting photoanodes. *RSC Adv.* **2016**, *6*, 80221–80225. [[CrossRef](#)]
98. Jeon, T.H.; Choi, S.K.; Jeong, H.W.; Kim, S.; Park, H. Photoelectrochemical water oxidation using ZnO nanorods coupled with cobalt-based catalysts. *J. Electrochem. Sci. Technol.* **2011**, *2*, 187–192. [[CrossRef](#)]
99. Sharma, V.; Kumar, P.; Shrivastava, J.; Solanki, A.; Satsangi, V.R.; Dass, S.; Shrivastav, R. Vertically aligned nanocrystalline Cu–ZnO thin films for photoelectrochemical splitting of water. *J. Mater. Sci.* **2011**, *46*, 3792–3801. [[CrossRef](#)]
100. Qiu, Y.; Yan, K.; Deng, H.; Yang, S. Secondary branching and nitrogen doping of ZnO nanotetrapods: Building a highly active network for photoelectrochemical water splitting. *Nano Lett.* **2012**, *12*, 407–413. [[CrossRef](#)] [[PubMed](#)]

101. Gupta, M.; Sharma, V.; Shrivastava, J.; Solanki, A.; Singh, A.P.; Satsangi, V.R.; Dass, S.; Shrivastav, R. Preparation and characterization of nanostructured ZnO thin films for photoelectrochemical splitting of water. *Bull. Mater. Sci* **2009**, *32*, 23–30. [[CrossRef](#)]
102. Bai, Z.; Yan, X.; Kang, Z.; Hu, Y.; Zhang, X.; Zhang, Y. Photoelectrochemical performance enhancement of ZnO photoanodes from ZnIn₂S₄ nanosheets coating. *Nano Energy* **2015**, *14*, 392–400. [[CrossRef](#)]
103. Wang, T.; Lv, R.; Zhang, P.; Li, C.; Gong, J. Au nanoparticle sensitized ZnO nanopencil arrays for photoelectrochemical water splitting. *Nanoscale* **2015**, *7*, 77–81. [[CrossRef](#)] [[PubMed](#)]
104. Hamid, S.B.A.; Teh, S.J.; Lai, C.W.; Perathoner, S.; Centi, G. Applied bias photon-to-current conversion efficiency of ZnO enhanced by hybridization with reduced graphene oxide. *J. Energy Chem.* **2016**, in press. [[CrossRef](#)]
105. Chen, H.M.; Chen, C.K.; Chang, Y.-C.; Tsai, C.-W.; Liu, R.-S.; Hu, S.-F.; Chang, W.-S.; Chen, K.-H. Quantum dot monolayer sensitized ZnO nanowire-array photoelectrodes: True efficiency for water splitting. *Angew. Chem. Int. Ed.* **2010**, *122*, 6102–6105. [[CrossRef](#)]
106. Kumari, B.; Sharma, S.; Satsangi, V.R.; Dass, S.; Shrivastav, R. Surface deposition of Ag and Au nano-isles on ZnO thin films yields enhanced photoelectrochemical splitting of water. *J. Appl. Electrochem.* **2015**, *45*, 299–312. [[CrossRef](#)]
107. Abd Samad, N.A.; Lai, C.W.; Abd Hamid, S.B. Influence applied potential on the formation of self-organized ZnO nanorod film and its photoelectrochemical response. *Int. J. Photoenergy* **2016**, *2016*, 1413072. [[CrossRef](#)]



© 2017 by the authors. Licensee MDPI, Basel, Switzerland. This article is an open access article distributed under the terms and conditions of the Creative Commons Attribution (CC BY) license (<http://creativecommons.org/licenses/by/4.0/>).